Loaded microwave cavity for compact vapor-cell clocks

Loaded microwave cavity for compact vapor-cell clocks

Michele Gozzelino, Salvatore Micalizio, Claudio E. Calosso, Aldo Godone, Haixiao Lin and Filippo Levi

Vapor-cell devices based on microwave interrogation provide a stable frequency reference with a compact and robust setup. Further miniaturization must focus on optimizing the physics package, containing the microwave cavity and atomic reservoir. In this paper, we present a compact cavity-cell assembly based on a dielectric-loaded cylindrical resonator. The loaded cavity resonating at 6.83 GHz has an external volume of only $35\,\mathrm{cm}^3$ and accommodates a vapor cell with $0.9\,\mathrm{cm}^3$ inner volume. The proposed design aims at strongly reducing the core of the atomic clock, maintaining at the same time high-performing short-term stability ($\sigma_y(\tau) \leq 5 \times 10^{-13}\,\tau^{-1/2}$ standard Allan deviation). The proposed structure is characterized in terms of microwave field uniformity and atom-field coupling with the aid of finite-elements calculations. The thermal sensitivity is also analyzed and experimentally characterized. We present preliminary spectroscopy results by integrating the compact cavity within a rubidium clock setup based on the pulsed optically pumping technique. The obtained clock signals are compatible with the targeted performances. The loaded-cavity approach is thus a viable design option for miniaturized microwave clocks.

I. Introduction

Vapor-cell atomic clocks provide excellent frequency stability together with low volume and power consumption. They are employed both on ground and in space applications [1]. Laser-based devices, working either with continuous or pulsed schemes, have shown state-of-the-art stability levels in their class, making them attractive options for next-generation global navigation systems [2–4]. Several industries have shown increasing interest for the pulsed optically pumped (POP) Rb clock, in virtue of its demonstrated performances and mature technology [5].

For industrial and spaceborne applications, a compact and light physics package is of high importance, not only for weight and volume considerations, but also for the possibility to reduce the overall power consumption and to improve the mechanical design. Moreover, for space applications, the mid and long-term stability is of greater relevance than having state-of-the-art short-term performances ($\simeq 1.5 \times 10^{-13}\,\tau^{-1/2}$) [6,7]. The development of a compact physics package goes in this direction, providing easier temperature stabilization and mitigation of temperature gradients, compared to a distributed object. This results in foreseen improved mid-term frequency stability performances [8].

M. Gozzelino, S. Micalizio, C. E. Calosso, A. Godone, and F. Levi are with Istituto Nazionale di Ricerca Metrologica, INRIM, Torino, Italy. The authors acknowledge support from the GSTP contract GSTP6.2 AO7935: *Rb POP Atomic Clock* funded by the European Space Agency.
E-mail: s.micalizio@inrim.it

H. Lin is with Key Laboratory of Quantum Optics, Shanghai Institute of Optics and Fine Mechanics, Chinese Academy of Sciences, Shanghai 201800 and with University of Chinese Academy of Sciences, Beijing 100049, China. Lin H. acknowledges the China Scholarship Council (CSC) and the National Natural Science Foundation of China (NSFC) under Grant No. 91536220.

This work presents a miniaturized microwave cavity suitable for POP [9–11] or continuous-wave [7] Rb clocks, looking for a trade-off between physical dimensions and desired short-term stability performances.

The physics package of Rubidium standards typically presents a layered structure, including several layers of magnetic and thermal shields. To reach an overall reduction of the package size, the most efficient strategy is to reduce the volume of the physical core of the clock, i.e. the microwave cavity. Many high-performing clocks make use of a cylindrical cavity resonant on the TE_{011} mode, because of its favorable $\mathbf{H}$-field distribution that is uniform and parallel to the longitudinal axis in the central region of the cavity. These features guarantee to excite the clock transition in an efficient way, increasing the contrast of the clock signal [12]. The cavity inner dimensions are designed in order to tune the TE_{011} resonance frequency to the atomic clock transition ($6.83\,\mathrm{GHz}$ for $^{87}\mathrm{Rb}$).

One way to shrink the cavity size, keeping the magnetic field resonant with the atomic clock transition, is the use of a loop-gap resonator (also called "magnetron" or "split-ring" resonator) [13,14]. This approach has been proven effective both for the continuous-wave and for the POP rubidium frequency standards [15–17]. Indeed, it provided a reduction of the overall cavity-cell volume up to a factor 4.5, maintaining cell size and clock performances comparable to those obtained with a traditional cylindrical cavity.

Alternatively, inserting a dielectric material inside the cavity volume can lead to a remarkable volume reduction [18,19]. Also, dielectric loading can be exploited, to some extent, to increase the field uniformity in the active volume [20].

We propose a novel design solution for the cavity-cell assembly based on an alumina-loaded microwave cavity, demonstrating an external volume of only $35\,\mathrm{cm}^3$. The loaded cavity still works on a TE_{011}-like mode, ensuring favorable magnetic field uniformity and directionality. The inner cavity volume is reduced by a factor 10 with respect to the unloaded design. Such a strong size reduction is made possible by scaling also the clock cell, whose inner volume is reduced by a factor 8. As demonstrated in more detail in Section II and Section III, this volume reduction partially affects the clock short-term stability, but still provides interesting performances.

The proposed alumina-loaded cavity offers new design alternatives and thus facilitates the use of the POP technology for in-field applications. Advantages of this approach are the notable size reduction and the mechanical stability, as the dielectric can also serve as a self-centering spacer for the clock cell.

The paper is organized as follows: in Section II the proposed design is introduced. In Section II-A the loaded-cavity main

features are analyzed with the aid of Finite Element Method (FEM) analysis. Finally, in Section III the cavity is experimentally characterized, and the expected short-term stability performances for such a cavity in a POP clock experiment are discussed.

II. Cylindrical loaded-cavity design

In this section, we present the mechanical design of the proposed cavity-cell assembly prototype, starting from the choice of the materials up to the final geometric configuration.

The target frequency of the microwave resonator working on the TE_{011} mode is the $^{87}\mathrm{Rb}$ clock frequency (6.83 GHz) for a foreseen operational temperature close to 65 °C. The cell is made of fused silica (dielectric constant $\epsilon = 3.8$), a material with small microwave losses ($\tan\delta = 1 \times 10^{-4}$) and low thermo-dielectric coefficient ($\beta = 10\,\mathrm{ppm/K}$). The chosen material for the loading dielectric is alumina (Al_2O_3). High-purity alumina has low dielectric losses ($\tan\delta < 1 \times 10^{-4}$) and high dielectric constant ($\epsilon \simeq 10$) [21]. A cavity completely filled with alumina and resonating at 6.8 GHz with the TE_{011} mode would have an inner volume of only $5\,\mathrm{cm}^3$, compared to $150\,\mathrm{cm}^3$ of an empty cylindrical cavity. The miniaturization capabilities are thus evident. Clearly, the cavity needs to accommodate a vapor cell with reasonable size, therefore a compromise between size reduction and expected clock performance must be found.

As it will be further discussed in Section II-A, to achieve significant volume reduction preserving at the same time the microwave field uniformity, the cell volume has been scaled, keeping roughly a factor 2 between the cavity and cell dimensions. The final size of the cell is set to have an internal diameter $2R = 10\,\mathrm{mm}$ and internal length $L = 10\,\mathrm{mm}$; the cavity has internal diameter $2a = 23\,\mathrm{mm}$ and length $d = 24\,\mathrm{mm}$.

Reducing the cell size has two effects: first, it reduces the available atomic sample volume, thus decreasing the atom number and the signal-to-noise ratio. Second, atomic population and coherence relaxation rates are increased, due to the collisions with the cell walls. The first point is not critical for many laser-based vapor-cell clocks, since they are not limited by shot-noise, rather from laser intensity and frequency noises [22]. The second issue can be mitigated by finding an optimal buffer gas pressure for which the total relaxation rate is minimized. Indeed, since for typical operational temperatures the main transverse relaxation-rate contribution is due to spin-exchange collisions between Rb atoms, there is margin to increase the pressure of the buffer gas without significantly enhancing the total relaxation rate [23].

Given the last considerations, for a traditional buffer-gas mixture composed of Ar and N_2 (1.6:1 ratio) [24], the total buffer-gas pressure is set to 40 Torr (53.2 hPa). At this pressure, and for a typical operational temperature of 65 °C, the transverse relaxation rate γ_2 is minimized ($\gamma_2 \simeq 450\,\mathrm{s}^{-1}$) [25]. Compared to the case of a $2\,\mathrm{cm} \times 2\,\mathrm{cm}$ cylindrical cell with 25 torr of buffer gas ($\gamma_2 = 320\,\mathrm{s}^{-1}$), this corresponds to a 1.4 times increase in the transverse relaxation rate. The γ_2 rate causes a decay of the atomic signal, ultimately limiting

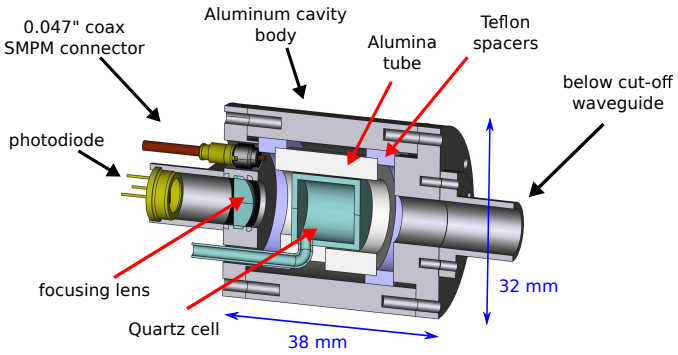

Fig. 1: Rendering of the cavity-cell assembly (cross-section view).

the maximum interrogation time T (usually T is set in such a way that $T \approx \gamma_2^{-1}$), so we expect the optimal Ramsey time to be reduced roughly by the same factor ($T \simeq 2.4\,\mathrm{ms}$ instead of $T \simeq 3.4\,\mathrm{ms}$). Finally, a reduction of the interrogation time lowers the atomic line quality factor, impacting the short-term stability. We consider these values a reasonable trade-off between expected performance and physics package size reduction.

The complete setup is shown in Fig. 1. The alumina loading dielectric has a cylindrical shape to preserve as much as possible the symmetry of the system. A small indent is introduced to allow the cell stem to exit the cavity volume (a cold point is desirable to induce metallic rubidium condensation outside the cavity volume). The alumina tube is centered with the aid of two Teflon (PTFE) rings that increase the mechanical tolerance. The cavity is made of aluminum and consists of a cylindrical body and two endcaps fixed by a set of screws. The end-caps of the cavity present two circular apertures, with 9 mm diameter, for optical access. These apertures are followed by cylindrical wave-guides with the same diameter. With such a geometry, the TE_{011} mode frequency is below the waveguide cut-off frequency and a power attenuation of at least 40 dB for the evanescent microwave field is obtained with a total waveguide length of 12 mm, making the clock frequency instability due to microwave leakage negligible. Also in this case, the reduction of the cell size and consequently of the needed optical access, allowed us to scale the waveguides volume maintaining the same attenuation of the unloaded design. On one side of the cavity, a magnetic coupling loop (created with a short-circuited SMPM coaxial cable) provides the microwave excitation. The system is completed with a plano-convex lens which focuses the laser light onto a $2.6\,\mathrm{mm} \times 2.6\,\mathrm{mm}$ Si photodiode.

A. Finite element analysis (FEA)

The resonance frequency and spatial distribution of the cavity modes of interest are analyzed with the aid of the finite-element-method software tool CST-studio [26].

A preliminary analysis has been conducted on the loaded cavity without the clock cell. This has allowed us to better characterize the properties of the employed alumina ceramic

TABLE I: Resonance frequencies and intrinsic Q-factors for the main cavity modes from the FEM simulations (assuming $\epsilon = 9.4$, $\tan\delta = 0.0001$ for the alumina and $\sigma = 3.8 \times 10^7\,\mathrm{S\,m^{-1}}$) for the electrical conductivity of Al. The cavity is loaded with Teflon and alumina only, without the clock cell. The experimental values have been measured at room temperature ($22.5\,^\circ\mathrm{C}$) by looking at the reflected microwave power from the loaded cavity in the frequency range of interest.

mode	ν_0 (FEA)[1]	Q_i (FEA)	ν_0 (exp.)	Q_i (exp.)
TE_{011}	$7.17\,\mathrm{GHz}$	5200	$7.00(1)\,\mathrm{GHz}$	4000 ± 200
TM_{111}	$7.58\,\mathrm{GHz}$	5100	$7.50(1)\,\mathrm{GHz}$	3200 ± 200
TM_{011}	$6.20\,\mathrm{GHz}$	4200	–	–

and to validate the simulations with fewer free parameters. From the results of the simulations, it is possible to label the main cavity modes from their spatial distribution. Moreover, the comparison of the simulated eigenfrequencies and Q-factors with the experimentally measured values can give additional information about the electrical properties of the employed alumina ceramic.

In Table I the resonance frequency of the TE_{011} mode and of the two nearest-neighbor modes are shown, together with their intrinsic quality factors. The latter are derived considering volume losses (from the dielectric) and wall losses (from the aluminum cavity). From the FEM analysis, given their spatial distribution, the two nearest modes are recognized as the TM_{011} and TM_{111}. They lie at least $400\,\mathrm{MHz}$ away from the eigenmode of interest for the clock operation. Conveniently, the dielectric loading completely lifts the degeneracy of the TM_{111} and TE_{011} modes, thus no mode-choke for the TM_{111} mode is necessary [12]. Table I also shows the frequency and Q-factors obtained experimentally. The measured quality factors are lower than the simulated ones, due to non-ideal conductivity and surface imperfections of the aluminum cavity walls and dielectric losses higher than expected. A discrepancy in the absolute frequencies is also observed, mainly attributed to the value of the dielectric constant of the alumina around $7\,\mathrm{GHz}$, which resulted $5\,\%$ higher than the value given from the manufacturer [27]. For this reason, in the rest of the discussion and in the following FEA calculations we assume $\epsilon = 9.9$ for the alumina, instead of the nominal value $\epsilon = 9.4$.

The subsequent part of the analysis focuses on the complete assembly, including the Teflon spacers, the $\mathrm{Al_2O_3}$ tube and the quartz cell. The effect of the quartz cell is to frequency shift the cavity modes by roughly $-130\,\mathrm{MHz}$ with respect to the values of Table I. The magnetic field distribution is also affected, even if the alumina plays the dominant role. Conversely, the Teflon spacers play a marginal role in terms of resonance frequency, as the relative shift induced on the cavity resonance is $\leq 1 \times 10^{-3}$. Their contribution is also negligible in terms of field distribution and losses, given the low dielectric constant of the material ($\epsilon_{\mathrm{PTFE}} = 2.1$) and the low magnitude of the electric field at the spacers location.

The main design guidelines are the uniformity and directionality grades of the TE_{011} mode (with respect to the quantization axis z). In particular, a "uniformity coefficient", introduced in [12], is used to characterize the amplitude variations of the H_z component over the active volume (V_a). To avoid ambiguity, the latter is taken coincident with the cell's inner volume. Compared to [12], the definition has been slightly modified to allow the maximum of the magnetic field to lie away from the center of the cavity (due to asymmetries in the cell and loading materials):

$$u = \frac{\frac{1}{V_a}\int_{V_a} H_z(\mathbf{r})^2\,dV}{\max\limits_{\mathbf{r}\in V_a}\{H_z(\mathbf{r})^2\}} \tag{1}$$

where $\mathbf{r}$ is the spatial coordinates vector. In this way $0 < u < 1$, with $u = 1$ corresponding to a perfectly uniform field distribution. Following [15], we also report the "orientation coefficient" ξ, defined as:

$$\xi = \frac{\int_{V_a} H_z(\mathbf{r})^2\,dV}{\int_{V_a} |\mathbf{H}(\mathbf{r})|^2\,dV} \tag{2}$$

This coefficient is a figure of merit of the orientation of the $\mathbf{H}$ field along the quantization axis. A high orientation factor (ξ close to 1) minimizes the excitation of the σ-transitions ($\Delta F = 1$, $\Delta m_F = \pm 1$), that can cause unwanted line-pulling on the clock transition [28]. For completeness, we also report the filling factor, which is mostly important for active oscillators (or POP clocks with microwave detection [29]), expressing the degree of coupling between the microwave field and the atomic sample:

$$\eta' = \frac{\left(\int_{V_a} H_z(\mathbf{r})\,dV\right)^2}{V_a \int_{V_c} |\mathbf{H}(\mathbf{r})|^2\,dV} \tag{3}$$

where V_c is the inner cavity volume. In Fig. 2a, the $\mathbf{H}$ field lines and amplitude for the proposed loaded-cavity assembly are shown in the y-z plane (the pumping/detection laser propagates along the z-axis). Rather good uniformity of the field component over the cell volume is observed. It should be noticed that along this plane we have the maximum field distortion due to the presence of the stem, whereas on the x-z plane the uniformity improves.

In Table II the previously introduced coefficients for the proposed configuration are reported and compared to other cavity-cell assemblies present in the literature. We can observe that the uniformity is increased compared to the case of the traditional cylindrical cavity while the orientation is comparable to other kinds of compact assemblies. Finally, the filling factor is reduced compared to the case of the unloaded cavity, reducing cavity-induced sensitivities such as cavity-pulling, but still high enough to provide sufficient coupling between the field and the atomic sample to achieve efficient clock interrogation. As a further term of comparison, in Table II we also report the external cavity volume for the various configurations.

B. Thermal sensitivity

For clock applications, the stability of the cavity mode frequency is of paramount importance, as it can impact the

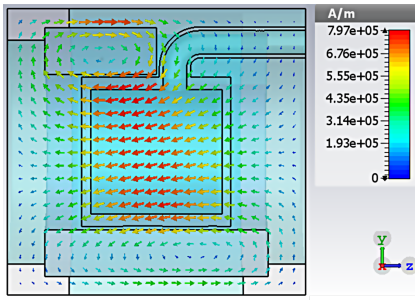

(a) **H** field in the y-z plane.

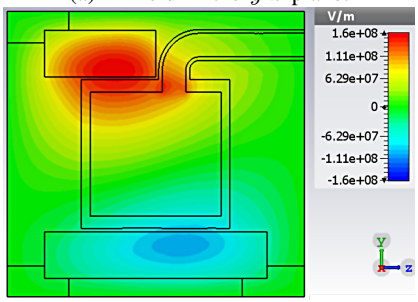

(b) E_x component in the y-z plane.

Fig. 2: Magnetic and electric field distributions inside the cavity volume for the TE_{011} mode.

TABLE II: Comparison of different published cavity-cell assemblies in terms of magnetic-field uniformity, orientation and filling factor. The external cavity volume is also reported.

cavity type	u	ξ	η'	external volume /cm^3
cylindrical [9,12]	0.59	0.92	0.38	130
magnetron [15]	n/a	0.87	0.14	44
magnetron [17]	n/a	0.90	n/a	30
Al_2O_3-loaded (this work)	0.82	0.76	0.20	35

clock frequency through cavity-pulling [23]. One of the main parameters of influence is temperature [12,30], which can change the resonance frequency ν_c by thermal expansion and by affecting the dielectric properties of the materials.

The total contribution to the sensitivity of the cavity resonance frequency to a temperature variation ΔT, for small variations from the operational setpoints, can be expressed as a sum of terms:

$$\frac{1}{\nu_c}\frac{\Delta\nu_c}{\Delta T} = \sum_k \frac{x_k}{\nu_c}\frac{\Delta\nu_c}{\Delta x_k}\alpha_k + \sum_i \frac{\epsilon_i}{\nu_c}\frac{\Delta\nu_c}{\Delta\epsilon_i}\beta_i \qquad (4)$$

where x_k are the geometric dimensions of the cavity and loading materials and $\alpha_k = \frac{\Delta x_k}{x_k \Delta T}$ the corresponding linear thermal expansion coefficient; ϵ_i is the dielectric constant of the i-th material inside the cavity and $\beta_i = \frac{\Delta\epsilon_i}{\epsilon_i \Delta T}$ the related thermo-dielectric coefficient.

In Table III the major contributions to the cavity frequency thermal sensitivity are expressed in relative terms. The sensitivity coefficients ($\frac{\Delta\nu_c}{\Delta x_k}$ and $\frac{\Delta\nu_c}{\Delta\epsilon_i}$) are taken from FEM calculations considering the complete assembly (alumina, Teflon,

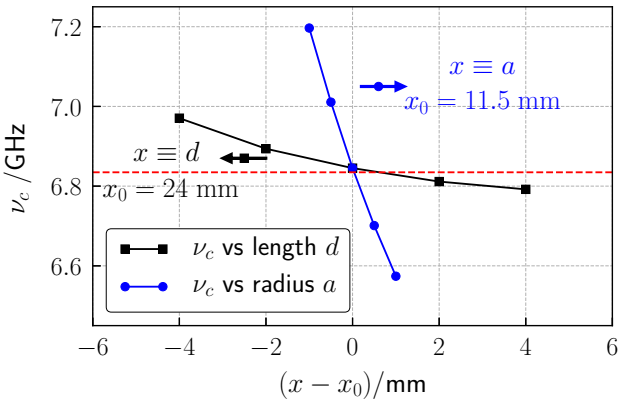

Fig. 3: TE_{011} resonance frequency as a function of cavity length and radius, at room temperature, as derived from the finite element analysis. The red dashed line corresponds to the atomic frequency (6.8347 GHz).

clock cell). In fact, this analysis can provide a numerical evaluation of the mode frequency as a function of the various parameters. In Fig. 3, for example, the TE_{011}-mode frequency is plotted as a function of the cavity length and radius.

Close to the working points, we find that the main contribution from variations of the geometric parameters is due to the cavity radius: $\frac{1}{\nu_c}\frac{\Delta\nu_c}{\Delta T} = -23.9\,\mathrm{ppm/K}$. The sensitivity to the cavity thermal expansion is -1.11, close to the case of the empty cylindrical cavity (equal to -1). Given the low thermal-expansion coefficient of alumina ($\alpha_{Al_2O_3} = 6.9\,\mathrm{ppm/K}$) [27]), the geometric contribution from the loading material is instead small ($\simeq -2\,\mathrm{ppm/K}$).

The other major contribution to the temperature sensitivity

TABLE III: Major contributions to the cavity thermal sensitivity expressed in relative terms. The geometric and thermo-dielectric contributions are listed in the upper and lower part of the table respectively, in decreasing order of importance.

x_k contribution	$\frac{x_k}{\nu_c}\frac{\Delta\nu_c}{\Delta x_k}$	α_k (ppm/K)	$\frac{1}{\nu_c}\frac{\Delta\nu_c}{\Delta T}$ (ppm/K)
cavity radius	-1.04	23	-23.9
cavity length	-0.07	23	-1.6
Al_2O_3 thickness	-0.16	6.9	-1.1
Al_2O_3 length	-0.07	6.9	-0.5
ϵ_i contribution	$\frac{\epsilon_i}{\nu_c}\frac{\Delta\nu_c}{\Delta\epsilon_i}$	β_i (ppm/K)	
Al_2O_3	-0.42	92	-38.8
fused silica	-0.03	10	-0.3
Total sensitivity			-66.2

Fig. 4: Loaded cavity components prior to the assembly. In the picture it is also shown the first cylindrical thermal shield. As a dimensional reference, a 10 euro cent coin is shown.

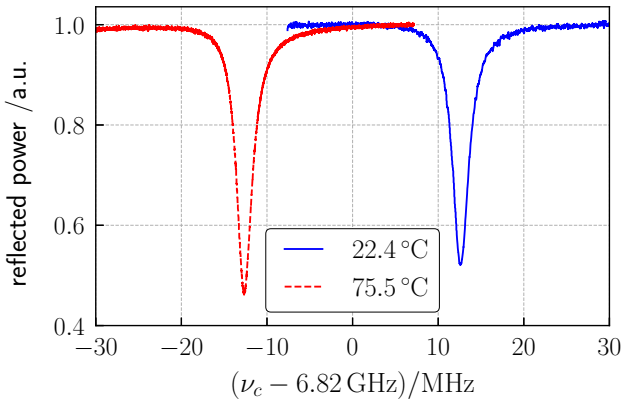

Fig. 5: TE_{011} resonance frequency for the complete assembly at two limit temperatures (ambient temperature and 75.5 °C), prior to fine tuning. The plot shows the power reflected from the cavity.

comes from the variation of the dielectric constant of the alumina. From the manufacturer's datasheet [27] we extract a thermo-dielectric coefficient $\beta_{Al_2O_3} = 92\,\mathrm{ppm/K}$ and from the FEM analysis we obtain a linear dependence of the cavity frequency on ϵ, with a slope $\frac{\epsilon}{\nu_c}\frac{\Delta\nu_c}{\Delta\epsilon} = -0.43$. This value is close to the case of a cavity fully loaded with alumina (-0.5). This is expected, since the electric field is mostly concentrated in the alumina volume. The contribution from the linear expansion of the fused-silica cell and effects related to the Teflon spacers are instead negligible ($< 0.1\,\mathrm{ppm/K}$).

Adding up all terms, the cavity resonance sensitivity is expected to be: $\Delta\nu_c/\Delta T = -453\,\mathrm{kHz/K}$. The total sensitivity to temperature is higher than the one of the unloaded cavity by almost a factor 3, but considering the lower filling factor (and for a typical cavity detuning of $500\,\mathrm{kHz}$ and loaded quality factor $Q_L = 2800$) we estimate an expected clock fractional frequency sensitivity to temperature of $\simeq 5 \times 10^{-12}/\mathrm{K}$ from cavity-pulling effect [23]. A temperature control at the level of $0.5\,\mathrm{mK}$ is thus sufficient to reach state-of-the-art stability performance in the 10^{-15} region. We remind that given the small size of the cavity, such a level of temperature stabilization is not hard to achieve.

III. Experimental characterization

The cavity-cell components are shown in Fig. 4 during the assembly phase. The cell used in the experimental validation is made of fused silica, with internal diameter and length both equal to $1\,\mathrm{cm}$, filled with isotopically enriched $^{87}\mathrm{Rb}$ and an Ar-N_2 buffer gas mixture (1.6:1 partial pressures ratio).

The loaded cavity resonance frequency has been experimentally measured by looking at the reflected power while sweeping the microwave frequency. The measured frequency at the operational temperature of 65 °C is found to be $22\,\mathrm{MHz}$ lower than the $^{87}\mathrm{Rb}$ atomic frequency, in reasonable agreement with the simulations (see Fig. 3). A fine tuning has been achieved by adjusting the cavity length by fractions of $1\,\mathrm{mm}$. A measurement of the cavity resonance frequency at different temperatures led to an experimental temperature coefficient of $-473\,\mathrm{kHz/K}$ for the untuned cavity and of $-461\,\mathrm{kHz/K}$ for the tuned cavity, in good agreement with the simulations.

No significant degradation of the cavity intrinsic quality factor has been observed in the range 25 °C to 70 °C, due to excess deposition of metallic Rb. Indeed, Q_i has a value of 3600 at room temperature, decreasing to 3200 around 70 °C. In Fig. 5 the loaded-cavity resonance mode is shown for two limit temperatures. The measurements refer to the cavity resonance previous to the fine tuning. From this measurement we can also determine the cavity coupling parameter β [29], which has a value of 0.2.

The proposed cavity-cell assembly has been tested with a POP clock scheme. The cavity has been operated at ambient pressure, integrated into an existing structure (same as in [31]) composed of 2 layers of thermal shielding and 3 layers of magnetic shielding. A static quantization magnetic field lifts the Zeeman degeneracy and isolates the clock transition. The optics package is the one described in [9], including a distributed feedback laser (DFB) working on the D_2 line, frequency stabilized with an external reference cell through saturated absorption spectroscopy. The laser frequency is tuned to the minimum of the clock cell absorption profile for the $|F = 2\rangle$ atomic ground-state. The pulsing is provided by an amplitude-modulated acousto-optic modulator operating in single-pass configuration. The system is completed with a low-noise digital control and acquisition system [32] and the microwave synthesis chain presented in [33].

To validate the simulations performed in Section II-A, following the method introduced in [15], we performed spectroscopy of the σ-transitions $|F_g = 1, m_F = 0\rangle \rightarrow |F_g = 2, m_F = \pm 1\rangle$. The interrogation is performed with a Rabi pulse in the microwave domain and the pulse area is chosen to be equal to $\frac{\pi}{2}$ for the clock transition ($|F_g = 1, m_F = 0\rangle \rightarrow |F_g = 2, m_F = 0\rangle$). The atomic population is detected with a weak laser probe pulse, with the usual absorption scheme. The result is shown in Fig. 6. From the excitation probabilities of the three transitions we can retrieve the relative magnitude of the corresponding Rabi frequencies (that we can call Ω_π, Ω_{σ_+} and Ω_{σ_-}). Finally, since the Rabi

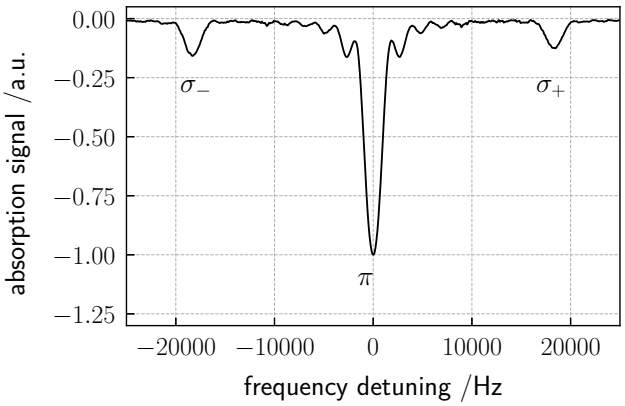

Fig. 6: Zeeman transitions for a quantization magnetic field of 2.7 µT. The spectroscopy is performed with a Rabi interrogation scheme. From the relative excitation probabilities the orientation factor ξ can be estimated.

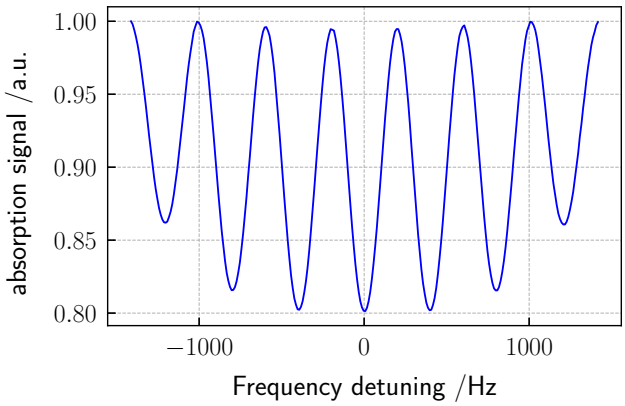

Fig. 7: Ramsey scan of the atomic line (absorption signal as a function of the microwave detuning from the atomic frequency; each data point is the result of 3 averages). Cavity temperature 64.5 °C, free-evolution time $T = 2.0\,\mathrm{ms}$, Rabi pulses length $t_1 = 0.4\,\mathrm{ms}$.

frequency is proportional to the **H**-field amplitude, we define the experimental orientation coefficient ξ_{exp} as:

$$\xi_{exp} = \frac{\Omega_\pi^2}{\Omega_\pi^2 + \Omega_{\sigma_-}^2 + \Omega_{\sigma_+}^2} \tag{5}$$

The value of ξ_{exp} is found to be 0.77, in good agreement with the simulations.

In Fig. 7 a scan of the Ramsey fringes, obtained with a laser absorption measurement as the microwave frequency is swept, is shown. The total cycle time is 3.35 ms, including pumping, clock interrogation and detection. The free-evolution time T is equal to 2 ms, while the Rabi pulses are 0.4 ms long. The laser beam is collimated with a gaussian $1/e^2$ diameter of 6 mm. The pumping power is 4 mW, for a pulse duration of 0.4 ms. The detection pulse power and duration are 200 µW and 0.15 ms respectively. With such timings and parameters, we obtained a fringe contrast of about 20 %.

To characterize the atomic properties of the Rb sample in the clock cell, we measured the longitudinal relaxation time T_1, directly accessible with an optical detection of the population evolution, with the Franzen method [34,35]. By this means we get $T_1 = 1.7(2)\,\mathrm{ms}$ at 64.5 °C. The transverse relaxation time T_2 is inferred by comparing envelope of the experimental Ramsey fringes to the one computed with the theory developed in [36]. From this analysis, it turns out that T_2 is roughly 10 % lower than T_1, corresponding to $\gamma_2 \simeq 650\,\mathrm{s}^{-1}$.

The shift induced on the clock transition by the buffer gas is $+8555(5)$ Hz, consistent with a total buffer gas pressure of 49(2) Torr, assuming negligible error on the buffer gas composition [24].

Finer tuning of the clock operating parameters (optical power, beam waist, cycle time, etc...) is needed, seeking for the ultimate stability performances. However, a stability below 5×10^{-13} at 1 s is compatible with the clock signal shown in Fig. 7, considering the major noise sources of the current setup (including laser RIN and frequency noise, detector noise, etc...). This estimate is confirmed by preliminary measurements and will be further characterized in future works.

IV. Conclusions

A compact cavity-cell assembly based on high-grade purity alumina as loading material has been designed, realized and characterized in terms of the main parameters of interest for microwave clock applications. The dielectric loading has led to a reduction of a factor 10 of the inner cavity volume, compared to the traditional cylindrical cavity. The size reduction was achieved by maintaining the favorable field uniformity of the TE_{011} mode and high cavity quality factor.

Despite the scaling of the clock cell dimension, introduced to push the miniaturization, we achieved high fringe contrast and high atomic-line quality factor by integrating the cavity in a POP clock setup. The obtained clock signal is compatible with a high-performing vapor-cell Rb clock, with short-term in the mid $10^{-13}\,\tau^{-1/2}$, as shown by preliminary characterization. The reduced size of the assembly facilitates thermal uniformity, with foreseen benefits in the medium-long term stability.

The loaded-cavity approach is thus a valid design option for the realization of compact vapor cell clocks based on microwave interrogation. As shown in [30], more refined configurations can also be studied to make the design even more robust against environmental sensitivities. In this paper, we reported a quality factor rather high for the POP with optical detection. If needed, this value can be tailored by using alumina with different percentages of impurities.

The proposed loaded-cavity assembly paves the way for a strongly miniaturized Rb-clock physics package with low mass and low power consumption, particularly appealing for spaceborne applications.

ACKNOWLEDGMENTS

The authors thank Elio K. Bertacco for precious technical help and Marwan S.p.A. (Pisa, Italy) for the cell filling. We acknowledge valuable input on the alumina production process from Jörg-Uwe Wichert from Wesgo Ceramics (Erlangen, Germany) and Wesgo Ceramics GmbH for the alumina pieces procurement. We also thank the LED laboratory staff from Politecnico di Torino for providing the CST software and computational facility.

REFERENCES

[1] W. J. Riley, *A History of the Rubidium Frequency Standard*. IEEE UFFC-S History, 2019.

[2] A. Godone, F. Levi, C. E. Calosso, and S. Micalizio, "High-performing vapor-cell frequency standards," *Riv. Nuovo Cimento*, vol. 38, pp. 133–171, Mar. 2015.

[3] J. C. Camparo and T. U. Driskell, "The mercury-ion clock and the pulsed-laser rubidium clock: Near-term candidates for future GPS deployment," Aerospace Corporation, Tech. Rep. TOR-2015-03893, 2015.

[4] B. L. Schmittberger and D. R. Scherer, "A review of contemporary atomic frequency standards," 2020, arXiv:2004.09987.

[5] P. Arpesi, J. Belfi, M. Gioia, N. Marzoli, R. Romani, A. Sapia, M. Gozzelino, C. Calosso, F. Levi, S. Micalizio, A. Tuozzi, and M. Belloni, "Rubidium pulsed optically pumped clock for space industry," in *2019 Joint Conference of the IEEE International Frequency Control Symposium and European Frequency and Time Forum (EFTF/IFC)*. IEEE, apr 2019.

[6] S. Micalizio, A. Godone, C. Calosso, F. Levi, C. Affolderbach, and F. Gruet, "Pulsed optically pumped rubidium clock with high frequency-stability performance," *IEEE Trans. Ultrason., Ferroelectr., Freq. Control*, vol. 59, no. 3, pp. 457–462, mar 2012.

[7] T. Bandi, C. Affolderbach, C. Stefanucci, F. Merli, A. K. Skrivervik, and G. Mileti, "Compact high-performance continuous-wave double-resonance rubidium standard with $1.4 \times 10^{-13}\ \tau^{-1/2}$ stability," *IEEE Trans. Ultrason., Ferroelectr., Freq. Control*, vol. 61, no. 11, pp. 1769–1778, November 2014.

[8] A. Hudson and J. Camparo, "Mesoscopic physics in vapor-phase atomic systems: Collision-shift gradients and the 0-0 hyperfine transition," *Phys. Rev. A*, vol. 98, no. 4, oct 2018.

[9] S. Micalizio, C. E. Calosso, A. Godone, and F. Levi, "Metrological characterization of the pulsed Rb clock with optical detection," *Metrologia*, vol. 49, no. 4, p. 425, 2012.

[10] N. Almat, M. Gharavipour, W. Moreno, F. Gruet, C. Affolderbach, and G. Mileti, "Long-term stability analysis toward $< 10^{-14}$ level for a highly compact POP Rb cell atomic clock," *IEEE Trans. Ultrason., Ferroelectr., Freq. Control*, vol. 67, no. 1, pp. 207–216, jan 2020.

[11] Q. Shen, H. Lin, J. Deng, and Y. Wang, "Pulsed optically pumped atomic clock with a medium- to long-term frequency stability of 10^{-15}," *Rev. Sci. Instrum.*, vol. 91, no. 4, p. 045114, apr 2020.

[12] A. Godone, S. Micalizio, F. Levi, and C. Calosso, "Microwave cavities for vapor cell frequency standards," *Rev. Sci. Instrum.*, vol. 82, no. 7, p. 074703, jul 2011.

[13] W. Froncisz and J. S. Hyde, "The loop-gap resonator: a new microwave lumped circuit ESR sample structure," *J. Magn. Reson.*, vol. 47, no. 3, pp. 515–521, may 1982.

[14] T. Sphicopoulos and F. Gardiol, "Slotted tube cavity: a compact resonator with empty core," *IEE Proceedings H - Microwaves, Antennas and Propagation*, vol. 134, no. 5, p. 405, 1987.

[15] C. Stefanucci, T. Bandi, F. Merli, M. Pellaton, C. Affolderbach, G. Mileti, and A. K. Skrivervik, "Compact microwave cavity for high performance rubidium frequency standards," *Rev. Sci. Instrum.*, vol. 83, no. 10, p. 104706, oct 2012.

[16] S. Kang, M. Gharavipour, C. Affolderbach, F. Gruet, and G. Mileti, "Demonstration of a high-performance pulsed optically pumped rb clock based on a compact magnetron-type microwave cavity," *J. Appl. Phys.*, vol. 117, no. 10, p. 104510, mar 2015.

[17] Q. Hao, W. Xue, W. Li, F. Xu, X. Wang, W. Guo, P. Yun, and S. Zhang, "Microwave pulse-coherent technique based clock with a novel magnetron-type cavity," *IEEE Trans. Ultrason., Ferroelectr., Freq. Control*, vol. 67, no. 4, pp. 873 – 878, 2019.

[18] D. A. Howe and F. L. Walls, "A compact hydrogen maser with exceptional long-term stability," *IEEE Trans. Instrum. Meas.*, vol. 32, no. 1, pp. 218–223, mar 1983.

[19] H. E. Williams, T. M. Kwon, and T. McClelland, "Compact rectangular cavity for rubidium vapor cell frequency standards," in *37th Annual Symposium on Frequency Control*, June 1983, pp. 12–17.

[20] K. Wang, Z. Du, Z. Yu, Y. Tian, Y. Liu, and S. Zhang, "A novel kind of microwave cavity with low temperature sensitivity and high uniformity for POP rubidium frequency standards," in *2019 Joint Conference of the IEEE International Frequency Control Symposium and European Frequency and Time Forum (EFTF/IFCS)*, apr 2019.

[21] D. D. Marco, K. Drissi, N. Delhote, O. Tantot, P.-M. Geffroy, S. Verdeyme, and T. Chartier, "Dielectric properties of pure alumina from 8 GHz to 73 GHz," *J. Eur. Ceram. Soc.*, vol. 36, no. 14, pp. 3355–3361, 2016.

[22] C. E. Calosso, M. Gozzelino, A. Godone, H. Lin, F. Levi, and S. Micalizio, "Intensity detection noise in pulsed vapor-cell frequency standards," *IEEE Trans. Ultrason., Ferroelectr., Freq. Control*, vol. 67, no. 5, pp. 1074–1079, 2020.

[23] S. Micalizio, A. Godone, F. Levi, and C. Calosso, "Pulsed optically pumped ^{87}Rb vapor cell frequency standard: A multilevel approach," *Phys. Rev. A*, vol. 79, p. 013403, Jan 2009.

[24] J. Vanier, R. Kunski, N. Cyr, J. Y. Savard, and M. Têtu, "On hyperfine frequency shifts caused by buffer gases: Application to the optically pumped passive rubidium frequency standard," *J. Appl. Phys.*, vol. 53, no. 8, pp. 5387–5391, 1982.

[25] J. Vanier and C. Audoin, *The Quantum Physics of Atomic Frequency Standards*. Adam Hilger, 1989.

[26] https://www.3ds.com/products-services/simulia/products/cst-studio-suite/.

[27] *AL995^{TM} datasheet*, Morgan Advanced Materials, WESGO Ceramics GmbH.

[28] V. Gerginov, N. Nemitz, and S. Weyers, "Initial atomic coherences and ramsey frequency pulling in fountain clocks," *Phys. Rev. A*, vol. 90, no. 3, sep 2014.

[29] A. Godone, S. Micalizio, and F. Levi, "Pulsed optically pumped frequency standard," *Phys. Rev. A*, vol. 70, no. 2, aug 2004.

[30] N. R. Wang, R. F. Yang, T. Z. Zhou, and L. S. Gao, "Frequency–temperature compensated sapphire loaded cavity for compact hydrogen masers," *Metrologia*, vol. 45, no. 5, pp. 534–538, sep 2008.

[31] C. Calosso, S. Micalizio, A. Godone, E. Bertacco, and F. Levi, "Electronics for the pulsed rubidium clock: Design and characterization," *IEEE Trans. Ultrason., Ferroelectr., Freq. Control*, vol. 54, no. 9, pp. 1731–1740, sep 2007.

[32] C. E. Calosso, M. Gozzelino, E. Bertacco, S. Micalizio, B. François, and P. Yun, "Generalized electronics for compact atomic clocks," in *2017 Joint Conference of the European Frequency and Time Forum and IEEE International Frequency Control Symposium (EFTF/IFCS)*, July 2017, pp. 322–323.

[33] B. François, C. E. Calosso, M. Abdel Hafiz, S. Micalizio, and R. Boudot, "Simple-design ultra-low phase noise microwave frequency synthesizers for high-performing Cs and Rb vapor-cell atomic clocks," *Rev. Sci. Instrum.*, vol. 86, no. 9, p. 094707, 2015.

[34] W. Franzen, "Spin relaxation of optically aligned rubidium vapor," *Phys. Rev.*, vol. 115, no. 4, pp. 850–856, aug 1959.

[35] M. Gharavipour, C. Affolderbach, F. Gruet, I. S. Radojičić, A. J. Krmpot, B. M. Jelenković, and G. Mileti, "Optically-detected spin-echo method for relaxation times measurements in a Rb atomic vapor," *New J. Phys.*, vol. 19, no. 6, p. 063027, 2017.

[36] S. Micalizio, C. E. Calosso, F. Levi, and A. Godone, "Ramsey-fringe shape in an alkali-metal vapor cell with buffer gas," *Phys. Rev. A*, vol. 88, no. 3, sep 2013.